Environmental Science Nano

Ligand removal energetics control CO2 electroreduction selectivity on atomically precise, ligated alloy nanoclusters

Journal:	*Environmental Science: Nano*
Manuscript ID	EN-ART-02-2022-000157.R1
Article Type:	Paper

Ligand removal energetics control CO_2 electroreduction selectivity on atomically precise, ligated alloy nanoclusters

Malena Rybacki, Anantha Venkataraman Nagarajan, Giannis Mpourmpakis*

Department of Chemical and Petroleum Engineering, University of Pittsburgh, Pittsburgh, Pennsylvania 15261, USA

*Corresponding Author email: gmpourmp@pitt.edu

Keywords: heterometal doping, CO formation, hydrogen evolution, active sites

Environmental Significance Statement

The room temperature electrocatalytic conversion of CO_2 (greenhouse gas) using various metal nanoclusters is a promising approach to sustainably produce valuable fuels and chemicals. Here, using a combination of theory and computation, we systematically explore the effect of doping atomically precise, ultra-small nanoclusters (~1nm) to enable the enhanced design of active and selective CO_2 conversion catalysts. Along with elucidating the effect of dopant type and location, we introduce a descriptor-based approach that can be generalized across all alloy nanoclusters to help identify new nanomaterials with improved catalytic properties. Overall, results from this work can help circumvent time consuming experimentation and computation, resulting in a materials design framework that advances a circular economy.

Abstract

Atomically precise, thiolate-protected gold nanoclusters (TPNCs) exhibit remarkable catalytic performance for the electrochemical reduction of carbon dioxide (CO_2R) to CO. The origin of their high CO_2R activity and selectivity has been attributed to partial ligand removal from the thiolate-covered surfaces of TPNCs to expose catalytically active sulfur atoms. Recently, heterometal doped (alloy) TPNCs have been shown to exhibit enhanced CO_2R activity and selectivity compared to their monometallic counterparts. However, systematic studies on the effect of doping (metal type and location on TPNC) on active site exposure and CO_2R activity are missing in literature. Herein, we apply Density Functional Theory calculations to investigate the effect of heterometal (Pt, Pd, Hg and Cd) doping of $Au_{25}(SR)_{18}$ TPNC on the active site exposure and CO_2R activity and selectivity. We reveal that doping significantly modifies relevant

TPNC electronic properties, such as electron affinity, while also altering partial ligand removal and carboxyl (*COOH) intermediate formation energies. Furthermore, we demonstrate that changing the dopant (e.g. Hg) position can change the selectivity of the TPNC towards $CO_{(g)}$ or $H_{2(g)}$ formation, highlighting the importance of dopant locations in TPNC-based CO_2R. Most notably, we report a universal (i.e. capturing different dopant types and positions) linear trend between the ligand removal energy and i) the *COOH formation energy, as well as, ii) the hydrogen (*H) formation energy on the different alloy TPNCs. Thus, utilizing the ligand removal energy as a descriptor for CO_2RR activity and selectivity, our work opens new avenues for accelerated computational screening of different alloy TPNCs for electrocatalytic CO_2R applications.

Introduction

Since the industrial revolution, atmospheric CO_2 concentrations have increased steadily by 0.28 ppm per year[1], leading to an increase in global temperature that is projected to be unsustainable for the long term health of the planet due to the greenhouse effect. Consequently, interest in room temperature electrocatalytic reduction of CO_2 (CO_2R) has increased, with the greenhouse gas CO_2 being a source to sustainably generate fuels and chemicals[2, 3]. For many years, metal nanoparticles (NPs)[4, 5] have been investigated as CO_2R catalysts—most notably, Au-based NPs due to their high selectivity towards $CO_{(g)}$ formation[6-10]. $CO_{(g)}$ is a valuable product of the CO_2R reaction as it can be used as feedstock for chemical transformations in industry, such as in the production of liquid hydrocarbons through the Fischer–Tropsch process[11]. However, owing to the polydispersity in size, the determination of active sites on the surface of NPs is challenging[12]. To overcome this challenge, thiolate-protected Au nanoclusters (TPNCs) are ideal systems to gain mechanistic understanding of CO_2R pathways due to their atomic precision and exact structures, which are determined by single crystal X-ray diffraction[13]. Their structures are commonly represented by the formula $Au_n(SR)_m^q$ with n and m denoting the exact number of Au atoms and stabilizing ligands respectively and q being the overall charge possessed by the TPNC. The structure of TPNCs is known to comprise of a metallic core surrounded by a hybrid thiolate (metal-organic) shell[14]. From a catalysis perspective, TPNCs have consistently displayed higher CO_2R performance (activity and selectivity) than larger Au NPs[15-19]. Recent studies have attributed the high activity and selectivity to partial-ligand (-R removal) or full-ligand removal (-SR removal) from the surface of TPNCs, leading to the exposure of catalytically active S or Au atoms respectively[20-22]. Specifically, -R removal was shown to be thermodynamically more preferrable than –SR removal and interestingly, S sites were shown to be more

active and selective for CO_2R to $CO_{(g)}$. This is due to the lower formation energy of the important carboxyl (*COOH) intermediate on the S sites, which is often known to be the rate-limiting intermediate for CO_2R on Au-based catalysts[21]. We note that hydrogen evolution reaction (HER) competes with CO_2R at experimentally applied overpotentials, with hydrogen (*H) formation energy commonly used as a descriptor for HER activity.

Heterometal doping of nanostructures has been widely utilized as a promising strategy to tailor and improve CO_2R performance[23]. More recently, extensive experimental efforts have enabled the controlled synthesis of heterometal doped TPNCs with a single dopant atom such as Pd[17], Pt[24], Cd[25] and Hg[26] being incorporated into the structure of TPNCs. Heterometal doping modifies the electronic structure of TPNCs while retaining nanocluster stability essential for CO_2R, resulting in enhanced catalytic performance[27, 28]. For example, doping a single atom (monodoping) of Pd or Pt into $Au_{25}(SR)_{18}$ (abbreviated as Au_{25}) results in the significant reduction of the highest occupied molecular orbital (HOMO) - lowest unoccupied molecular orbital (LUMO) gap (0.32 eV for Pd-doped Au_{25} and 0.29 eV for Pt-doped Au_{25}) compared to the HOMO-LUMO gap of their monometallic Au_{25} counterpart (1.32 eV)[23, 25, 29]. Here, Pd and Pt were experimentally determined to be located in the center of the 13-atom metallic icosahedral core. On the contrary, monodoping of Cd and Hg into Au_{25}, while resulting in changes to the electronic fingerprint (UV-vis spectrum) of the TPNC, does not lead to drastic reductions in the HOMO-LUMO gap[26, 30]. The experimentally determined position of Cd and Hg is on the outer surface of the metallic core and shell of the TPNCs, respectively. At the same time, we acknowledge that determining the location of Hg via experiments can be challenging (due to the similarity between Au and Hg), with previous reports suggesting that Hg can exist either on the outer surface[25] of the metallic core or on the shell[26]. Considering the results from Yao et al., Hg is likely to exist on the shell[26]. Owing to their ultra-small size, TPNCs exhibit quantum confinement effects, making the dopant location as well as type of type of dopant crucial factors that can significantly alter TPNC electronic properties[23]. Focusing on their application as electrocatalysts for CO_2 reduction[12, 31-33], an ideal dopant would decrease the thermodynamic barriers associated with ligand removal (for active site exposure) as well as stabilize the *COOH intermediate. Recently, numerous studies have demonstrated the high CO_2R performance of alloy TPNCs[6, 17, 24, 34]. However, many of these studies have focused on very specific systems, mostly comparing a monodoped TPNC to its monometallic precursor or counterpart. Thus, a crucial challenge in investigating the CO_2R performance of alloy TPNCs resides in systematically understanding dopant effects on CO_2R performance. Furthermore, heterometal doping of TPNCs vastly expands the materials domain[35], necessitating the need to develop accelerated methods for screening new, catalytically active alloy TPNCs[36]. Instead of performing computationally

intensive density functional theory (DFT) calculations for every possible TPNC along with challenging and expensive trial-and-error experiments, one can develop descriptor-based relationships based on select DFT calculations that can aid in the identification of new alloy TPNCs that are active and selective towards CO_2R.

Electron affinity (EA) and ionization potential (IP)[37, 38] of a TPNC measure the ability of a TPNC to accept or donate an electron respectively[39], and can potentially correlate with TPNC electrocatalytic behavior[40]. Moreover, EA and IP are electronic properties that can be calculated with relatively less computational expense compared to tedious DFT calculations that describe complete reaction pathways. Recently, the $Ag_2Au_{36}(SR)_{18}$ TPNC exhibited improved HER activity compared to the monometallic $Au_{38}(SR)_{24}$, with the improved activity attributed to a lower *H binding energy and higher EA associated with $Ag_2Au_{36}(SR)_{18}$[40]. Herein, we analyze global electronic properties such as EA and IP of various Au_{25}-based alloy TPNCs using 4 different dopants (Pt, Pd, Hg, Cd). We also investigate the effect of dopant position on thermodynamic barriers for partial ligand (-R) removal, as well as *COOH and *H formation. We find that Hg doped Au_{25} (Hg in the experimentally determined location-shell of the TPNC) exhibits the lowest ligand removal energy (LRE) but highest *COOH formation energy (CFE). Interestingly, we observe an opposite trend when Hg is in the central position of the icosahedral core, with the resulting hypothetical Hg doped Au_{25} exhibiting the highest LRE but lowest CFE. Thus, we reveal that changing the dopant location alone can switch the selectivity of an alloy TPNC towards $CO_{(g)}$ or $H_{2(g)}$ formation, highlighting the importance of TPNC dopant location in the overall CO_2R behavior. Importantly, we demonstrate that regardless of dopant location or type, a linear trend exists between LRE and CFE across the entire series of alloy TPNCs. We further show that LREs correlate with *H formation energies (HFEs), resulting in a weaker linear trend between CFE and HFE. This work can guide optimal CO_2R TPNC catalyst design by elucidating the interplay between active site exposure and CO_2R performance, using LREs as a descriptor for CO_2R activity and selectivity.

Methodology

DFT calculations were performed using the PBE functional[41] and DZVP basis set[42] in conjunction with GTH pseudopotentials[43] as implemented in the CP_2K[44] software. This level of theory is computationally tractable and accurately captures electronic and CO_2R catalytic properties of TPNCs[6, 17, 20, 21]. A total of twelve different alloy TPNCs were investigated using Au_{25} as the parent structure (see **Fig. 1** for structure of fully optimized Au_{25}). Au_{25} was chosen due to its well-known symmetrical structure that allows for clear investigation of dopant locations either in the core or the shell[45]. Four different dopants, namely Pd, Pt,

Hg and Cd were chosen due their synthetic accessibility into the structure of Au_{25} to form $PdAu_{24}$, $PtAu_{24}$, $CdAu_{24}$ and $HgAu_{24}$[26, 29, 30]. Of note, heterometal doping of Au_{25} with these 4 dopants does not change the total number of ligands or metal atoms in the TPNC, thus allowing us to compare electronic properties of all the TPNCs at the exact same size. The location of each dopant has been experimentally determined; Pt and Pd reside in the center of the icosahedral core[29], while Cd and Hg reside on the outer surface of the metallic core and hybrid metal-organic shell, respectively[26, 30]. To systematically understand the effect of dopant locations on CO_2R and recognize the ambiguity associated with the location of Hg, we considered the four dopants in all three distinct locations of Au_{25}: center of the icosahedral core (C), outer surface of the icosahedral core (OC) and shell of the TPNC (S). This results to 4 alloy TPNCs with the dopants in their experimentally determined locations and 8 hypothetical alloy TPNCs with dopants in the two other locations. All hypothetical alloy TPNCs are denoted by an asterisk (*). For example, a TPNC in which Cd is present in the center of the icosahedral core of Au_{25} is denoted as $Cd_{(C)}Au_{24}$*, whereas if Cd is present on the outer surface of the icosahedral core of Au_{25} (as experimentally determined), it is denoted as $Cd_{(OC)}Au_{24}$. The surface of each of the TPNCs was modeled with simplified -SCH_3 ligands instead of larger, experimentally used ligands, such as phenylethanethiol. Such an approximation reduces computational expense while accurately capturing geometric and electronic properties of TPNCs[28, 46]. The neutral (0) as well as the negatively (-1) charged Au_{25} was investigated since it is known to exist in both states[45]. All alloy TPNCs were studied in the neutral (0) charge state as per previous experimental observations[26, 29].

Geometry optimizations of all TPNCs were performed in a 30 x 30 x 30 $Å^3$ non-periodic unit cell until forces converged to a minimum of 0.01 eV $Å^{-1}$. Systems with an even number of electrons were considered to have a multiplicity of 1, whereas systems with an odd number of electrons were considered to have a multiplicity of 2 to account for unpaired electrons. After geometry optimization, EAs and IPs were calculated as per equation (1) and (2) respectively. The HOMO and LUMO of each TPNC was visualized using the VESTA[47] software package with an isosurface value of 0.015. The EA is calculated as the difference between the electronic energy of the TPNC with an extra electron and that of the TPNC in its original charge state (eq. 1). The IP is calculated as the difference between the electronic energy of the TPNC with one less electron and that of the TPNC in its original charge state (eq. 2). Equations (1) and (2) assume that the original charge state of the TPNC is 0 (all alloy TPNCs and Au_{25} in neutral charge state). A similar equation can be used to calculate the EA for Au_{25} that can also exist in a charge state of -1. A more negative EA implies greater preference for electron acceptance and a more positive IP implies less preference for electron donation.

$$EA = E_{NC}^{-1} - E_{NC}^{0} \ (1)$$

$$IP = E_{NC}^{+1} - E_{NC}^{0} \ (2)$$

The energy required to release the -R group (LRE) from the TPNC (to expose a sulfur active site) was calculated as per the equation (3):

$$LRE = \{E_{X_nAu_{25-n}S(SR)_{17}} + E_{RH(g)}\} - \{E_{X_nAu_{25-n}(SR)_{18}} + E_{H^+ + e^-}\} \ (3)$$

Each term represents the ground state electronic energy of each molecule or TPNC, with the first term representing the electronic energy of the -R removed TPNC and the third representing the electronic energy of the fully protected TPNC. 'n' is either 0 or 1 for the monometallic or alloy TPNCs respectively. X stands for Pt, Pd, Cd or Hg.

Additionally, the Gibbs free energy to form the *COOH intermediate (CFE) and *CO on the exposed S sites upon -R removal, was calculated as per equation (4) and (5):

$$CFE = \{G_{X_nAu_{25-n}SCOOH(SR)_{17}}\} - \{G_{X_nAu_{25-n}S(SR)_{17}} + G_{H^+ + e^-} + G_{co_{2(g)}}\} (4)$$

$$CO\ formation = \{G_{X_nAu_{25-n}SCO(SR)_{17}} + G_{H_2O_{(l)}}\} - \{G_{X_nAu_{25-n}SCOOH(SR)_{17}} + G_{H^+ + e^-}\} \ (5)$$

where each term represents the Gibbs free energy (G) of the molecule or TPNC at 298 K and 1 atm (typical electrochemical reaction conditions), with the first terms representing the G of the -R removed TPNC with *COOH (equation 4) and *CO (equation 5) adsorbed on the S active site. The second term in equation (4) represents the electronic energy of the -R removed TPNC. The vibrational modes of the adsorbates (*COOH and *CO), $H_{2(g)}$, $H_2O_{(l)}$ and $CO_{2(g)}$ molecules were considered to calculate the CFE or *CO formation energy. The computational hydrogen electrode[48] was employed to approximate the energy of a proton coupled electron transfer ($H^+ + e^-$) as ½ $H_{2(g)}$ in equations (3) and (4). Gas phase corrections to the $CO_{2(g)}$ and $H_{2(g)}$ molecules were also included according to Peterson and co-workers[49]. Noting that CO_2R takes place under aqueous environment, it is worth mentioning that previous studies[6, 21] have demonstrated the presence of water to slightly stabilize the *COOH intermediate by 0.1 eV – 0.2 eV. Importantly, solvent effects did not affect previously observed computational CO_2R trends on monometallic and alloy NCs, which followed the experimental trends. Thus, in this work, we focus on CO_2R modifications primarily associated with heterometal doping without the effect of solvation. Bader charge analysis[50] was carried out to obtain fractional charge distributions on the S active sites of TPNCs. Previous work[21, 51] has investigated the effect of exposing S from two distinct locations on the surface of Au_{25}, with one site (site

A) exhibiting lower thermodynamic barriers (by ~0.2 eV) for exposure as compared to the other (site B). For consistency, we choose to focus on the site that exhibits the lower thermodynamic barrier for exposure (site A). Lastly, we note that complete ligand (-SR) removal leading to exposure of metal sites could potentially also happen under reaction conditions[21, 24, 34]. However, previous work has shown that thermodynamic barriers for -R removal (exposure of surface S) is lower than -SR removal (exposure of metal)[6, 17, 21]. Moreover, S sites have been shown to be more active and selective for CO_2R[21, 22]. Thus, we only consider -R removed TPNCs in this work.

Results and Discussion

The different structural regions of Au_{25} TPNC are marked in **Fig. 1a**, with each region offering a distinct location for doping (C, OC or S). We optimized the structures of all 14 TPNCs in their fully protected and -R removed states. The structures (except the hypothetical ones) are identical to those obtained from experiments[26, 29, 30]. Additionally, the structural integrity of all TPNCs after -R removal was preserved after optimization (refer to **Fig. S1** for optimized structures of all fully protected and -R removed TPNCs). Next, we calculated EAs (**Fig. 1b**) and IPs (**Fig. 1c**) of all TPNCs in their fully protected (red bars) as well as -R removed states (blue bars). To maintain consistency, we compare the properties of all TPNCs in the neutral charge state (for EA and IP of Au_{25} in the (-1) charge state, refer to **Fig. S2**). As stated previously, it is hypothesized that EA and IP, a measure of a TPNC's ability to gain and lose an electron respectively could potentially correlate with its electrocatalytic performance[40]. We immediately observe that the dopants do not significantly change the IP (**Fig. 1c**) of any fully protected TPNC, while significantly altering their EA (**Fig. 1b**) in some cases. Specifically, we observe that when Cd and Hg are present in any of the three distinct locations, the EA of the resulting $Cd_{(C)}Au_{24}$*, $Cd_{(OC)}Au_{24}$, $Cd_{(S)}Au_{24}$*, $Hg_{(C)}Au_{24}$*, $Hg_{(OC)}Au_{24}$* and $Hg_{(S)}Au_{24}$ TPNCs is significantly lower (less exothermic; i.e. EA > -2.23 eV) than Au_{25} (EA=-2.89 eV). This means that the presence of Cd and Hg heterometal, decreases the affinity for accepting electrons in the alloy TPNCs compared to the monometallic Au. Interestingly, when Pd and Pt are present in the center of the icosahedral core of Au_{25}, the resulting $Pd_{(C)}Au_{24}$ and $Pt_{(C)}Au_{24}$ TPNCs roughly maintain their EA (-2.70 eV and -2.82 eV respectively) compared to Au_{25}. However, when present in the two other distinct positions, the EAs of the resulting $Pd_{(S)}Au_{24}$*, $Pd_{(OC)}Au_{24}$*, $Pt_{(S)}Au_{24}$* and $Pt_{(OC)}Au_{24}$* are much lower (EA > -2.39 eV) than Au_{25}. Furthermore, since we consider the -R removed TPNC as the active state of the catalyst during CO_2R, we calculate EAs and IPs of the TPNCs upon -R removal (blue bars). Interestingly, the EA of all alloy TPNCs increases upon -R removal (becomes more exothermic) but IPs remain relatively unchanged, suggesting that the -R removed (active state) of the TPNC is preferred for electron acceptance

than the fully protected TPNC during electrochemically reducing conditions. Specifically, we observe that $Cd_{(OC)}Au_{24}$, $Pt_{(C)}Au_{24}$ and $Pd_{(C)}Au_{24}$ upon -R removal exhibit highest EAs (-2.97 eV, -3.00 eV and -3.01 eV

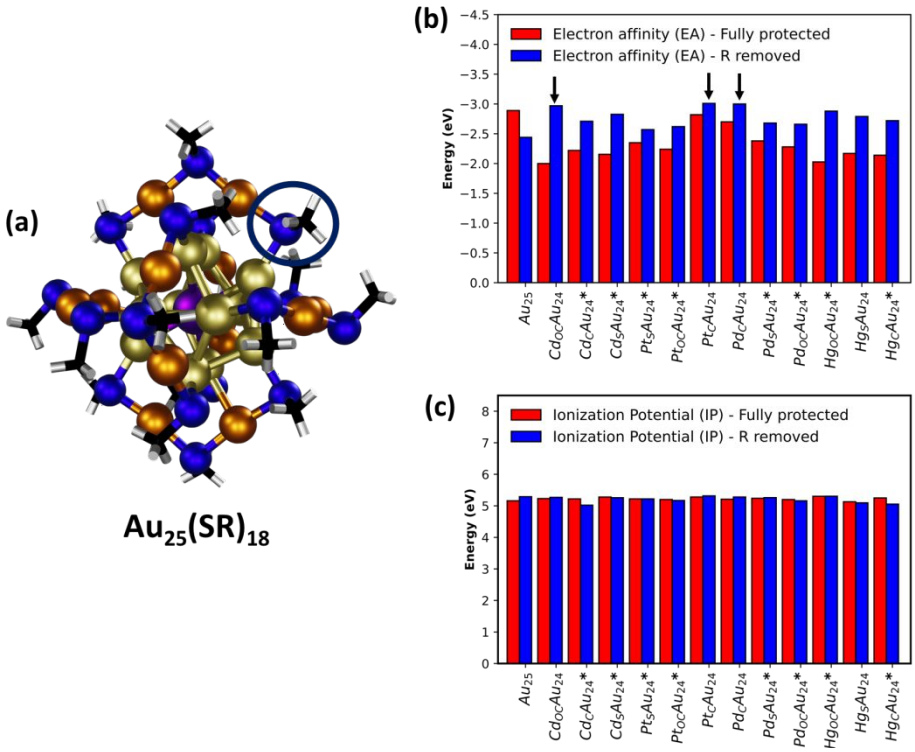

Figure 1. (a) Structure of fully protected Au_{25} TPNC. Color scheme: Purple - Au atom in the center of icosahedral core, Gold - Au atoms in the icosahedral core (except center), Orange - Au atoms in the shell, Blue - S, Black - C, Grey - H. Red circle denotes site of -R removal. (b) EA and (c) IP of TPNCs in their fully protected (red) and -R removed state (blue). Black arrows denote TPNCs with highest EA upon -R removal.

respectively, denoted by black arrows). This observation could potentially justify previous experiments and theory demonstrating the high CO_2R activity of $PdAu_{24}$ and Cd doped $Au_{23}(SR)_{16}$[6, 17]. Frontier orbitals such as the HOMO and LUMO are most relevant from a reactivity perspective since these participate in chemical bonds. Thus, we examined the effect of dopant position on these two orbitals of the TPNCs in their fully protected (**Fig. S3**) and -R removed states (**Fig. S4**). In general, we observe noticeable differences in the HOMOs and LUMOs of the fully protected TPNCs upon heterometal doping. Especially considering the hypothetical $Hg_{(C)}Au_{24}$* and $Cd_{(C)}Au_{24}$* with divalent Hg and Cd, we observe a greater contribution of the core atoms (Hg/Cd and Au) to the HOMO compared to the contribution of the core atoms to the HOMO of Au_{25}, $Pd_{(C)}Au_{24}$ and $Pt_{(C)}Au_{24}$. This increased contribution suggests relatively high localization of electron density in the core due to Hg and Cd doping in the central position of the core. Interestingly,

when we compare the HOMO of $Hg_{(S)}Au_{24}$, the contribution from the core atoms (only Au) to its HOMO is significantly less than that of $Hg_{(C)}Au_{24}$*, demonstrating the influence of heterometal doping in the core of the TPNC[17, 29]. Analysis of the HOMO and LUMO of TPNCs upon -R removal (**Fig. S4**) shows an increase in the contribution of the S active site to the HOMO of all TPNCs[21, 22]. This increase in contribution to the HOMO illustrates an increased reactivity of the active S sites on the surface of TPNCs towards the CO_2R intermediates. We especially note that $Hg_{(C)}Au_{24}$* exhibits relatively high electron density localization around the S active site, further suggesting the possibility of exhibiting favorable bonding with reaction intermediates compared to other alloy TPNCs. Bader charge also reveals a relative increase in the overall electron density on the S active sites of all TPNCs upon -R removal (**Table S1**).

*COOH formation on TPNCs is often known to be the limiting step during the electrochemical reduction of CO_2 to CO, resulting in the use of CFE as a descriptor for CO_2RR activity. **Fig. 2a** depicts the Gibbs free energy change (ΔG) to form the *COOH intermediate on the S active sites. It is apparent that the type of dopant as well as the location of the dopant play a significant role in the thermodynamics associated with *COOH formation. Specifically, we observe that the CFE on every single -R removed alloy TPNC except $Hg_{(S)}Au_{24}$ (0.94 eV) is lower than the monometallic Au_{25} (0.64 eV). The CFE on $Cd_{(C)}Au_{24}$* (0.17 eV), $Hg_{(C)}Au_{24}$* (0.13 eV), $Pt_{(S)}Au_{24}$* (0.19 eV) and $Pd_{(S)}Au_{24}$* (0.13 eV) is among the lowest in the series, making them the most active TPNCs. Importantly, we observe a drastic difference (0.80 eV) in the CFE on $Hg_{(C)}Au_{24}$* compared to $Hg_{(S)}Au_{24}$, illustrating the importance of dopant locations on CO_2R activity. Moreover, these results clearly show that even though dopant atoms can be present in the core that is

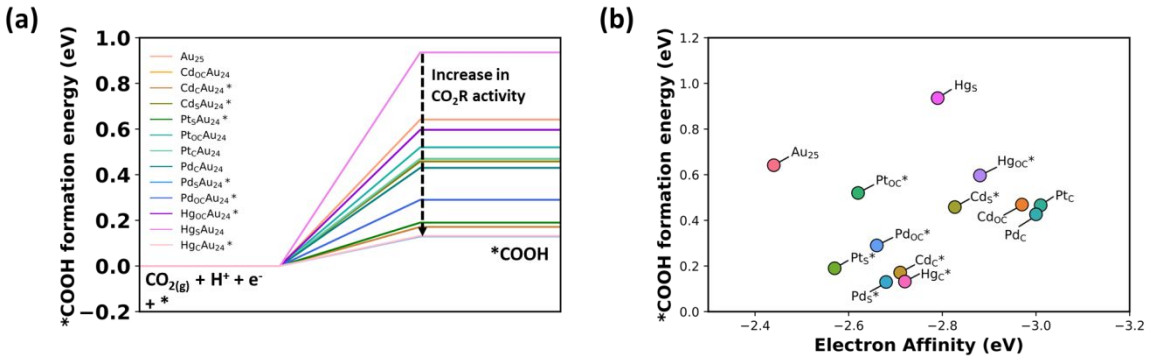

Figure 2. (a) *COOH formation energy on S active sites of TPNCs and (b) *COOH formation energy as a function of EA of -R removed TPNCs.

inaccessible during catalysis, they play a key role in the stabilization of reaction intermediates due to the small size of TPNCs. Taking into consideration EAs as a potential descriptor for screening

electrocatalytically active TPNCs, we attempt to build a correlation between the EA of -R removed TPNCs and CFE (**Fig. 2b**). Considering the most active TPNCs - $Cd_{(C)}Au_{24}$*, $Hg_{(C)}Au_{24}$*, $Pt_{(S)}Au_{24}$* and $Pd_{(S)}Au_{24}$*, we observe that none of these TPNCs exhibit the highest EAs in the series (-2.71 eV, -2.72 eV, -2.57 eV and -2.68 eV respectively). In fact, $Cd_{(S)}Au_{24}$* and $Hg_{(OC)}Au_{24}$* have higher EAs (-2.83 eV and -2.88 eV respectively) than $Cd_{(C)}Au_{24}$*, $Hg_{(C)}Au_{24}$*, $Pt_{(S)}Au_{24}$ and $Pd_{(S)}Au_{24}$*. At the same time, these two TPNCs also exhibit higher CFEs (0.46 eV and 0.60 eV respectively) and thus, it is apparent that a higher EA does not always correlate with a lower CFE. This implies that descriptors such as EA, which considers the electronic properties of the entire TPNC, might not be best suited to solely rationalize CO_2R activity of TPNCs. Noting this, we move to investigate bond energetics associated with active site exposure and *COOH formation to obtain localized descriptors for TPNC-based CO_2R. **Fig. 3a** depicts the energy required to expose the S active site (-R removal) from each TPNC (LRE). We observe a wide range of LREs that depend on the type of dopant and importantly, the location of the dopant. Interestingly, we observe $Cd_{(OC)}Au_{24}$ (-0.10 eV) along with $Pd_{(C)}Au_{24}$ (-0.12 eV) and $Pt_{(C)}Au_{24}$ (-0.12 eV) have similar LREs, a trend observed with their CFEs (0.47 eV, 0.47 eV and 0.43 eV respectively) as well (**Fig. 2a**). $Hg_{(S)}Au_{24}$ exhibits the most exothermic LRE of -0.51 eV and at the same time, $Hg_{(C)}Au_{24}$* exhibits the most endothermic LRE (0.10 eV, similar to

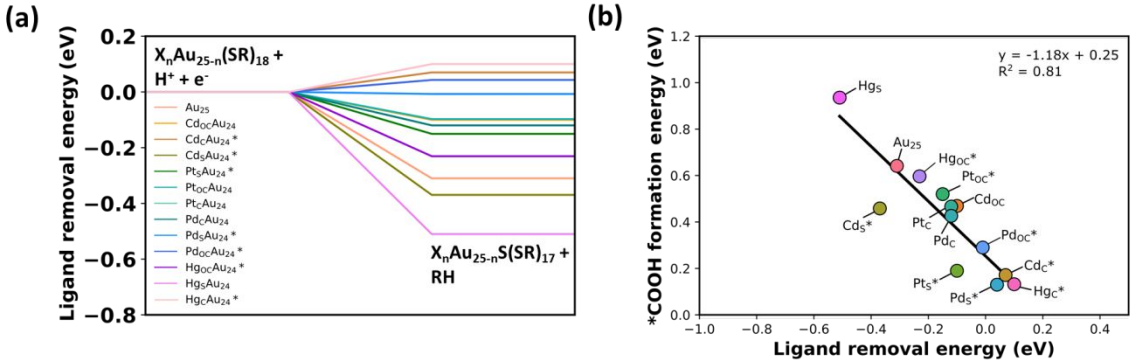

Figure 3. (a) Energy required for -R removal to expose S active sites on TPNCs. (b) *COOH formation energies as a function of ligand removal energies (LRE). R = CH_3.

$Cd_{(C)}Au_{24}$*). Especially considering the difference between the lowest and highest LREs on the different Cd and Hg TPNCs (0.44 eV and 0.61 eV respectively) compared to that of Pt and Pd TPNCs (0.05 eV and 0.16 eV respectively), it is clear that the position of divalent Cd and Hg significantly impacts the thermodynamics of active site exposure. This can be attributed to the higher charge redistribution associated with divalent metals, especially in the shell of the TPNC that results in the alteration of bond strengths around the active site. As mentioned earlier, owing to the similarity between Hg and Au, determining the location of Hg via experiments can be challenging and Hg has been shown to be present

either in OC or S[25, 26]. Interestingly, we note that $Hg_{(OC)}Au_{24}$* and $Hg_{(S)}Au_{24}$ show significantly different LREs and CFEs, highlighting the effect of dopant location during CO_2R. Interestingly, we observe that regardless of dopant type or position, there exists a negative linear correlation (**Fig. 3b**) between the LRE and CFE. In other words, more thermodynamically challenging active site exposure (more endothermic LRE) implies a lower CFE (higher CO_2R activity). Physically, this means that when the ligands on the TPNC surface are intact, the S-C bond strength is similar to the S-C bond strength when the *COOH intermediate is stabilized on S. This observation is consistent with previous work that has demonstrated the role of CO_2R reaction intermediates as stabilizing ligands under reaction conditions[16].

HER is known to compete with CO_2R under reaction conditions and thus, we also calculated the ΔG of *H formation to analyze the selectivity of the TPNCs investigated in this work. From a thermodynamics perspective, the qualitative descriptor for selectivity is known as the difference in limiting potentials (ΔU_L), which is the difference between the thermodynamically most challenging step between two reactions (CO_2R and HER in this case). For most TPNC based electrocatalytic studies (especially on Au_{25}), *COOH formation ($U_L CO_2R$) and *H formation ($U_L HER$) are known to be the limiting potentials for CO_2R and HER. A positive difference between $U_L CO_2R$ and $U_L HER$ implies selectivity towards $CO_{(g)}$ formation as opposed to $H_{2(g)}$ formation (see **Fig. S5** for ΔU_L of all TPNCs). **Fig. 4a** shows HFE as a function of LREs for all TPNCs. Similar to **Fig. 3b**, we notice a negative linear correlation between the HFE and LRE, implying that a lower LRE (more exothermic) not only correlates to higher HER activity (an ideal HER catalyst would have

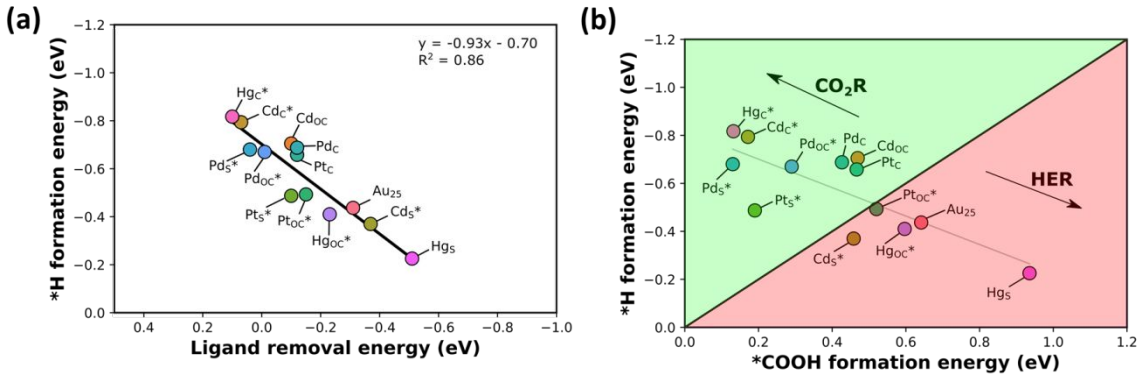

Figure 4. (a) *H formation energy on S active sites on TPNCs as a function of LRE. (b) *H formation energy as a function of *COOH formation energy. Green area contains TPNCs selective towards $CO_{(g)}$ while red area contains TPNCs selective towards $H_{2(g)}$. Grey line serves as a guide to the eye cutting across different selectivity regions (linear regression: y = -0.60x – 0.82, R^2 = 0.6).

HFE = 0 eV), but also to a lower (more negative) difference in limiting potential. For example, $Cd_{(S)}Au_{24}$ exhibits HFE of -0.37 eV while $Cd_{(OC)}Au_{24}$* exhibits HFE of -0.71 eV, leading to a ΔU_L of -0.09 eV for the

former and 0.24 eV for the latter. Comparing results from **Fig. 3b** and **4a**, we consequently obtain a weak linear behavior (R^2=0.6) between CFE and HFE (**Fig. 4b**) orienting the TPNCs in a line that cuts across different selectivity regions (forming $CO_{(g)}$ vs. $H_{2(g)}$ under reaction conditions). As it can be observed, all Pd doped Au_{25} TPNCs appear to be selective towards $CO_{(g)}$ while monometallic Au_{25} (in the 0 charge state) is selective towards $H_{2(g)}$. Interestingly, $Hg_{(C)}Au_{24}$* is selective towards $CO_{(g)}$ formation, while $Hg_{(OC)}Au_{24}$* and $Hg_{(S)}Au_{24}$ are selective towards $H_{2(g)}$ formation. This particular result highlights the importance of atomic precision in the synthesis of TPNCs, clearly demonstrating that dopant locations can significantly influence the selectivity of a catalyst. We note that the formation of the *H intermediate on S sites is highly exothermic compared to the formation of the *COOH intermediate on the same sites. If we consider $Pd_{(c)}Au_{24}$ with S sites to be saturated with *H, forming the *COOH intermediate from *H bound to S is thermodynamically uphill (1.11 eV, Fig. S6) compared to forming *COOH via proton coupled electron transfer ($H^+ + e^-$, 0.43 eV). In addition, forming $H_{2(g)}$ through the HER from the adsorbed *H state is an endothermic step (0.69 eV), which would need a higher energy input to overcome. Previous experiments (via gas chromatography) have confirmed the primary identity of products as $CO_{(g)}$ with significantly lower amounts of $H_{2(g)}$ generated during CO_2R. Thus, considering the thermodynamic limiting steps of the entire reaction pathway for CO_2R and HER along with previous experiments, we expect the S sites on the majority of NCs studied in this work to be active and selective towards CO_2R (Fig. S5). Lastly, we note that CO formation can be the limiting potential on certain TPNCs[6], so we calculated the Gibbs free energy required to form *CO from the *COOH intermediate for TPNCs that were selective towards $CO_{(g)}$ formation (green region in **Fig. 4b**). In most cases, *COOH formation was still deemed to be the limiting potential, with exceptions being $Hg_{(C)}Au_{24}$*, $Cd_{(C)}Au_{24}$* and $Pt_{(S)}Au_{24}$* (**Table S2**). The difference between *CO formation and *COOH formation on these three TPNCs was < 0.23 eV, implying comparable energetics for *COOH and *CO formation. More importantly, we observed that the selectivity of $Hg_{(C)}Au_{24}$*, $Cd_{(C)}Au_{24}$* and $Pt_{(S)}Au_{24}$* does not switch to $H_{2(g)}$ formation, although there are slight shifts in their ΔU_L value. Thus, using LREs as a descriptor, we can capture CO_2R activity as well as selectivity of alloy TPNCs. Importantly, we observe the linear trends to exist regardless of dopant type or location, implying that such relationships could be extended to other TPNC systems (including different dopant types and doping locations). We note that TPNCs possess structural and electronic complexity at varying size regimes that may be exacerbated by heterometal doping. However, the use of physically relevant descriptors such as LRE and CFE is a promising step towards developing universal trends that can be applicable to other TPNCs. This concept remains to be computationally tested, but previous work[52] on metallic NPs has shown that adsorption and catalytic behavior (e.g. similar to CFE and HFE) is directly related to the stability of active

sites on catalysts (e.g. similar to LRE). Finally, we note that although ligand removal is critical for activating TPNCs towards CO_2R, previous work has shown that reaction intermediates such as COOH, H and CO can act as stabilizing ligands during the electrocatalytic cycle and maintain the overall stability of TPNCs under reaction conditions[16].

Conclusions

In this work, electronic structure calculations were performed to elucidate the effect of dopant type and position on the CO_2R activity and selectivity of ultra-small alloy TPNCs. Electronic and thermodynamic properties such as electron affinity (EA), ionization potential (IP) and ligand removal energy (LRE) were calculated to connect with their electrocatalytic CO_2R activity and selectivity. While no clear correlation exists between EA and CO_2R activity, a linear correlation is obtained between LRE and carboxyl formation energy (CFE) as well as LRE and hydrogen formation energy (HFE). This demonstrates that dopant positions can clearly alter the thermodynamics of active site exposure (LRE), CO_2R activity and selectivity of TPNCs. Importantly, the linear trend is obtained regardless of dopant type and location on the investigated TPNCs. Owing to a similar linear trend that exists between LFE and CFE as well as LRE and HFE, a weak linear trend is obtained between CFE and HFE. A strong energetic balance between exposing active sites during electrocatalysis and forming important reaction intermediates (measure of CO_2R activity and selectivity) on alloy TPNCs is revealed, which is crucial for TPNC electrocatalyst discovery. This work introduces LRE as a descriptor for capturing CO_2R activity and selectivity, with applications in accelerated screening of alloy TPNCs for sustainable fuels and chemicals production.

Author contributions

M.R and A.V.N contributed equally to this work. G.M conceptualized and directed the work. All authors contributed to the preparation of the manuscript.

Conflicts of interest

Nothing to declare.

Acknowledgements

This work has been supported by the National Science Foundation (NSF, CBET-CAREER program) under Grant No. 1652694. Computational support has been provided by the Center for Research Computing (CRC) at the University of Pittsburgh and the National Energy Research Scientific Computing Center

(NERSC), a U.S. Department of Energy Office of Science User Facility operated under contract no. DE-AC02-05CH11231. The authors would like to thank Dr. Michael Cowan for fruitful technical discussions.

References

1. K. Hashimoto, in *Global Carbon Dioxide Recycling: For Global Sustainable Development by Renewable Energy*, ed. K. Hashimoto, Springer Singapore, Singapore, 2019, DOI: 10.1007/978-981-13-8584-1_3, pp. 5-17.
2. K. O. Yoro and M. O. Daramola, in *Advances in Carbon Capture*, eds. M. R. Rahimpour, M. Farsi and M. A. Makarem, Woodhead Publishing, 2020, DOI: https://doi.org/10.1016/B978-0-12-819657-1.00001-3, pp. 3-28.
3. X. Zhao, L. Du, B. You and Y. Sun, Integrated design for electrocatalytic carbon dioxide reduction, *Catalysis Science & Technology*, 2020, **10**, 2711-2720.
4. D. Gao, H. Zhou, J. Wang, S. Miao, F. Yang, G. Wang, J. Wang and X. Bao, Size-Dependent Electrocatalytic Reduction of CO2 over Pd Nanoparticles, *Journal of the American Chemical Society*, 2015, **137**, 4288-4291.
5. C. Kim, H. S. Jeon, T. Eom, M. S. Jee, H. Kim, C. M. Friend, B. K. Min and Y. J. Hwang, Achieving Selective and Efficient Electrocatalytic Activity for CO2 Reduction Using Immobilized Silver Nanoparticles, *Journal of the American Chemical Society*, 2015, **137**, 13844-13850.
6. S. Li, A. V. Nagarajan, D. R. Alfonso, M. Sun, D. R. Kauffman, G. Mpourmpakis and R. Jin, Boosting CO2 Electrochemical Reduction with Atomically Precise Surface Modification on Gold Nanoclusters, *Angew Chem Int Ed Engl*, 2021, **60**, 6351-6356.
7. Y. Chen, C. W. Li and M. W. Kanan, Aqueous CO2 Reduction at Very Low Overpotential on Oxide-Derived Au Nanoparticles, *Journal of the American Chemical Society*, 2012, **134**, 19969-19972.
8. S. Chen and A. Chen, Electrochemical Reduction of Carbon Dioxide on Au Nanoparticles: An in Situ FTIR Study, *The Journal of Physical Chemistry C*, 2019, **123**, 23898-23906.
9. Z. Wang, K. Sun, C. Liang, L. Wu, Z. Niu and J. Gao, Synergistic Chemisorbing and Electronic Effects for Efficient CO2 Reduction Using Cysteamine-Functionalized Gold Nanoparticles, *ACS Applied Energy Materials*, 2019, **2**, 192-195.
10. E. Andrews, S. Katla, C. Kumar, M. Patterson, P. Sprunger and J. Flake, Electrocatalytic Reduction of CO2at Au Nanoparticle Electrodes: Effects of Interfacial Chemistry on Reduction Behavior, *Journal of The Electrochemical Society*, 2015, **162**, F1373-F1378.
11. W. Zhou, K. Cheng, J. Kang, C. Zhou, V. Subramanian, Q. Zhang and Y. Wang, New horizon in C1 chemistry: breaking the selectivity limitation in transformation of syngas and hydrogenation of CO2 into hydrocarbon chemicals and fuels, *Chemical Society Reviews*, 2019, **48**, 3193-3228.
12. T. Higaki, Y. Li, S. Zhao, Q. Li, S. Li, X. S. Du, S. Yang, J. Chai and R. Jin, Atomically Tailored Gold Nanoclusters for Catalytic Application, *Angew Chem Int Ed Engl*, 2019, **58**, 8291-8302.
13. J. He, N. J. J. Johnson, A. Huang and C. P. Berlinguette, Electrocatalytic Alloys for CO2 Reduction, *ChemSusChem*, 2018, **11**, 48-57.
14. H. Hakkinen, M. Walter and H. Gronbeck, Divide and protect: capping gold nanoclusters with molecular gold-thiolate rings, *J Phys Chem B*, 2006, **110**, 9927-9931.
15. R. Jin, T. Higaki, Y. Li, S. Zhao, Q. Li, S. Li, X. Du, S. Yang and J. Chai, Atomically Tailored Gold Nanoclusters for Catalytic Application, *Angew Chem Int Ed Engl*, 2019, DOI: 10.1002/anie.201814156.
16. A. V. Nagarajan, R. Juarez-Mosqueda, M. J. Cowan, R. Jin, D. R. Kauffman and G. Mpourmpakis, Elucidating the stability of ligand-protected Au nanoclusters under electrochemical reduction of CO 2, *SN Applied Sciences*, 2020, **2**, 1-12.

17. S. Li, D. Alfonso, A. V. Nagarajan, S. D. House, J. C. Yang, D. R. Kauffman, G. Mpourmpakis and R. Jin, Monopalladium substitution in gold nanoclusters enhances CO2 electroreduction activity and selectivity, *ACS Catalysis*, 2020, **10**, 12011-12016.
18. S. Li, A. V. Nagarajan, Y. Li, D. R. Kauffman, G. Mpourmpakis and R. Jin, The role of ligands in atomically precise nanocluster-catalyzed CO 2 electrochemical reduction, *Nanoscale*, 2021, **13**, 2333-2337.
19. D. R. Kauffman, D. R. Alfonso, D. N. Tafen, C. Wang, Y. Zhou, Y. Yu, J. W. Lekse, X. Deng, V. Espinoza, J. Trindell, O. K. Ranasingha, A. Roy, J.-S. Lee and H. L. Xin, Selective Electrocatalytic Reduction of CO2 into CO at Small, Thiol-Capped Au/Cu Nanoparticles, *The Journal of Physical Chemistry C*, 2018, **122**, 27991-28000.
20. D. R. Alfonso, D. Kauffman and C. Matranga, Active sites of ligand-protected Au25 nanoparticle catalysts for CO2 electroreduction to CO, *J Chem Phys*, 2016, **144**, 184705.
21. N. Austin, S. Zhao, J. R. McKone, R. Jin and G. Mpourmpakis, Elucidating the active sites for CO2 electroreduction on ligand-protected Au25 nanoclusters, *Catalysis Science & Technology*, 2018, **8**, 3795-3805.
22. S. Zhao, N. Austin, M. Li, Y. Song, S. D. House, S. Bernhard, J. C. Yang, G. Mpourmpakis and R. Jin, Influence of Atomic-Level Morphology on Catalysis: The Case of Sphere and Rod-Like Gold Nanoclusters for CO2 Electroreduction, *ACS Catalysis*, 2018, **8**, 4996-5001.
23. X. Kang, Y. Li, M. Zhu and R. Jin, Atomically precise alloy nanoclusters: syntheses, structures, and properties, *Chem Soc Rev*, 2020, **49**, 6443-6514.
24. W. Choi, H. Seong, V. Efremov, Y. Lee, S. Im, D. H. Lim, J. S. Yoo and D. Lee, Controlled syngas production by electrocatalytic CO2 reduction on formulated Au25(SR)18 and PtAu24(SR)18 nanoclusters, *J Chem Phys*, 2021, **155**, 014305.
25. W. Fei, S. Antonello, T. Dainese, A. Dolmella, M. Lahtinen, K. Rissanen, A. Venzo and F. Maran, Metal Doping of Au25(SR)18(-) Clusters: Insights and Hindsights, *J Am Chem Soc*, 2019, **141**, 16033-16045.
26. C. Yao, Y. J. Lin, J. Yuan, L. Liao, M. Zhu, L. H. Weng, J. Yang and Z. Wu, Mono-cadmium vs Mono-mercury Doping of Au25 Nanoclusters, *J Am Chem Soc*, 2015, **137**, 15350-15353.
27. Y.-J. Liu, P. Shao, M.-Y. Gao, W.-H. Fang and J. Zhang, Synthesis of Ag-Doped Polyoxotitanium Nanoclusters for Efficient Electrocatalytic CO2 Reduction, *Inorganic Chemistry*, 2020, **59**, 11442-11448.
28. M. G. Taylor and G. Mpourmpakis, Rethinking Heterometal Doping in Ligand-Protected Metal Nanoclusters, *J Phys Chem Lett*, 2018, **9**, 6773-6778.
29. S. Tian, L. Liao, J. Yuan, C. Yao, J. Chen, J. Yang and Z. Wu, Structures and magnetism of mono-palladium and mono-platinum doped Au25(PET)18 nanoclusters, *Chem Commun (Camb)*, 2016, **52**, 9873-9876.
30. L. Liao, S. Zhou, Y. Dai, L. Liu, C. Yao, C. Fu, J. Yang and Z. Wu, Mono-Mercury Doping of Au25 and the HOMO/LUMO Energies Evaluation Employing Differential Pulse Voltammetry, *J Am Chem Soc*, 2015, **137**, 9511-9514.
31. S. Zhao, R. Jin and R. Jin, Opportunities and Challenges in CO2 Reduction by Gold- and Silver-Based Electrocatalysts: From Bulk Metals to Nanoparticles and Atomically Precise Nanoclusters, *ACS Energy Letters*, 2018, **3**, 452-462.
32. S. Li and R. Jin, in *Recent Advances in Nanoparticle Catalysis*, eds. P. W. N. M. van Leeuwen and C. Claver, Springer International Publishing, Cham, 2020, DOI: 10.1007/978-3-030-45823-2_2, ch. Chapter 2, pp. 39-68.
33. R. Jin, G. Li, S. Sharma, Y. Li and X. Du, Toward Active-Site Tailoring in Heterogeneous Catalysis by Atomically Precise Metal Nanoclusters with Crystallographic Structures, *Chem Rev*, 2021, **121**, 567-648.

34. S. Zhuang, D. Chen, L. Liao, Y. Zhao, N. Xia, W. Zhang, C. Wang, J. Yang and Z. Wu, Hard-Sphere Random Close-Packed Au47 Cd2 (TBBT)31 Nanoclusters with a Faradaic Efficiency of Up to 96 % for Electrocatalytic CO2 Reduction to CO, *Angew Chem Int Ed Engl*, 2020, **59**, 3073-3077.
35. M. J. Cowan and G. Mpourmpakis, Towards elucidating structure of ligand-protected nanoclusters, *Dalton Trans*, 2020, **49**, 9191-9202.
36. A. V. Nagarajan, D. J. Loevlie, M. J. Cowan and G. Mpourmpakis, Resolving electrocatalytic imprecision in atomically precise metal nanoclusters, *Current Opinion in Chemical Engineering*, 2022, **36**, 100784.
37. B. Sun and A. S. Barnard, The impact of size and shape distributions on the electron charge transfer properties of silver nanoparticles, *Nanoscale*, 2017, **9**, 12698-12708.
38. B.-R. Hyun, Y.-W. Zhong, A. C. Bartnik, L. Sun, H. D. Abruña, F. W. Wise, J. D. Goodreau, J. R. Matthews, T. M. Leslie and N. F. Borrelli, Electron Injection from Colloidal PbS Quantum Dots into Titanium Dioxide Nanoparticles, *ACS Nano*, 2008, **2**, 2206-2212.
39. M. J. Cowan, A. V. Nagarajan and G. Mpourmpakis, Correlating structural rules with electronic properties of ligand-protected alloy nanoclusters, *J Chem Phys*, 2021, **155**, 024303.
40. Y. Li, S. Li, A. V. Nagarajan, Z. Liu, S. Nevins, Y. Song, G. Mpourmpakis and R. Jin, Hydrogen Evolution Electrocatalyst Design: Turning Inert Gold into Active Catalyst by Atomically Precise Nanochemistry, *J Am Chem Soc*, 2021, **143**, 11102-11108.
41. J. P. Perdew, K. Burke and M. Ernzerhof, Generalized Gradient Approximation Made Simple, *Phys Rev Lett*, 1996, **77**, 3865-3868.
42. J. VandeVondele and J. Hutter, Gaussian basis sets for accurate calculations on molecular systems in gas and condensed phases, *J Chem Phys*, 2007, **127**, 114105.
43. S. Goedecker, M. Teter and J. Hutter, Separable dual-space Gaussian pseudopotentials, *Phys Rev B Condens Matter*, 1996, **54**, 1703-1710.
44. T. D. Kuhne, M. Iannuzzi, M. Del Ben, V. V. Rybkin, P. Seewald, F. Stein, T. Laino, R. Z. Khaliullin, O. Schutt, F. Schiffmann, D. Golze, J. Wilhelm, S. Chulkov, M. H. Bani-Hashemian, V. Weber, U. Borstnik, M. Taillefumier, A. S. Jakobovits, A. Lazzaro, H. Pabst, T. Muller, R. Schade, M. Guidon, S. Andermatt, N. Holmberg, G. K. Schenter, A. Hehn, A. Bussy, F. Belleflamme, G. Tabacchi, A. Gloss, M. Lass, I. Bethune, C. J. Mundy, C. Plessl, M. Watkins, J. VandeVondele, M. Krack and J. Hutter, CP2K: An electronic structure and molecular dynamics software package - Quickstep: Efficient and accurate electronic structure calculations, *J Chem Phys*, 2020, **152**, 194103.
45. X. Kang, H. Chong and M. Zhu, Au25(SR)18: the captain of the great nanocluster ship, *Nanoscale*, 2018, **10**, 10758-10834.
46. M. G. Taylor and G. Mpourmpakis, Thermodynamic stability of ligand-protected metal nanoclusters, *Nat Commun*, 2017, **8**, 15988.
47. K. Momma and F. Izumi, VESTA 3for three-dimensional visualization of crystal, volumetric and morphology data, *Journal of Applied Crystallography*, 2011, **44**, 1272-1276.
48. J. K. Nørskov, J. Rossmeisl, A. Logadottir, L. Lindqvist, J. R. Kitchin, T. Bligaard and H. Jónsson, Origin of the Overpotential for Oxygen Reduction at a Fuel-Cell Cathode, *The Journal of Physical Chemistry B*, 2004, **108**, 17886-17892.
49. A. A. Peterson, F. Abild-Pedersen, F. Studt, J. Rossmeisl and J. K. Nørskov, How copper catalyzes the electroreduction of carbon dioxide into hydrocarbon fuels, *Energy & Environmental Science*, 2010, **3**, 1311-1315.
50. G. Henkelman, A. Arnaldsson and H. Jónsson, A fast and robust algorithm for Bader decomposition of charge density, *Computational Materials Science*, 2006, **36**, 354-360.
51. J. McKay, M. J. Cowan, C. A. Morales-Rivera and G. Mpourmpakis, Predicting ligand removal energetics in thiolate-protected nanoclusters from molecular complexes, *Nanoscale*, 2021, **13**, 2034-2043.

52. J. Dean, M. G. Taylor and G. Mpourmpakis, Unfolding adsorption on metal nanoparticles: Connecting stability with catalysis, *Sci Adv*, 2019, **5**, eaax5101.